2019

Design Rules for Additive Manufacturing – Understanding the Fundamental Thermal Phenomena to Reduce Scrap

M. Reza Yavari

Kevin D. Cole

Prahalada K. Rao

Available online at www.sciencedirect.com

ScienceDirect

Procedia Manufacturing 33 (2019) 375–382

Procedia MANUFACTURING

www.elsevier.com/locate/procedia

16th Global Conference on Sustainable Manufacturing - Sustainable Manufacturing for Global Circular Economy

Design Rules for Additive Manufacturing – Understanding the Fundamental Thermal Phenomena to Reduce Scrap

M. Reza Yavari, Kevin D. Cole, Prahalada K. Rao*

Mechanical and Materials Engineering Department, University of Nebraska-Lincoln, Lincoln, NE 68588-0526, United States

Abstract

The goal of this work is to predict the effect of part geometry and process parameters on the direction and magnitude of heat flow – heat flux – in parts made using metal additive manufacturing (AM) processes. As a step towards this goal, the objective of this paper is to develop and apply the mathematical concept of heat diffusion over graphs to approximate the heat flux in metal AM parts as a function of their geometry. This objective is consequential to overcome the poor process consistency and part quality in AM. Currently, part build failure rates in metal AM often exceed 20%, the causal reason for this poor part yield in metal AM processes is ascribed to the nature of the heat flux in the part. For instance, constrained heat flux causes defects such as warping, thermal stress-induced cracking, etc. Hence, to alleviate these challenges in metal AM processes, there is a need for computational thermal models to estimate the heat flux, and thereby guide part design and selection of process parameters. Compared to moving heat source finite element analysis techniques, the proposed graph theoretic approach facilitates layer-by-layer simulation of the heat flux within a few minutes on a desktop computer, instead of several hours on a supercomputer.

Keywords: Additive Manufacturing, Heat Flux, Thermal Modeling, Heat Equation, Graph Theory, Discrete Approximation.

* Corresponding author. Tel.: +01-402-472-3458; fax: +01-402-472-1465.
E-mail address: rao@unl.edu

10.1016/j.promfg.2019.04.046

1. Introduction

The goal of this work is to understand the effect of process parameters and part design on the heat flux, i.e., the magnitude and direction of heat flow in metal parts, as they are being deposited (printed) layer-by-layer using metal additive manufacturing (AM) processes, such as laser powder bed fusion (LPBF) and directed energy deposition (DED) [1]. In pursuit of this goal, the objective of this paper is to develop and apply a graph theoretic approach to approximate the heat flux in metal AM parts. The motivating reasons for this research are two-fold [2].

In metal AM, the physio-mechanical properties of the part, such as its geometric integrity and microstructure, are governed by thermal process phenomena [1, 2]. These thermal aspects of the process are in turn entwined with the part design, support structure, and process parameters [1]. However, optimizing the design and process parameters in AM using statistical experimentation methods is prohibitively expensive given the small batch sizes in AM and the slow nature of the process compared with conventional manufacturing [3]. Furthermore, more than 50 process parameters are reported in LPBF alone it is not viable to investigate the effect of all these parameters using designed experiments. Hence, to narrow the experimental parameter set, a quantitative approach based on fundamental understanding of the thermal physics to understand the effect of part design and process parameters is needed [4-8].

Accurate quantitative approaches based on finite element analysis (FEA) have been successfully developed and applied for understanding the thermal aspects of AM at the part-level [9]. However, these pioneering non-proprietary approaches reported in the published literature are computationally expensive, with simulation of a few deposited layers amounting to many hours of computation on a super computer. Hence, newer approaches are needed to approximate the heat flux in a computationally efficient manner given different part designs and process parameters. In the context of FEA-modeling, we note that certain commercial, proprietary approaches that leverage adaptive meshing principles have drastically reduced the computational time [10, 11].

2. The Graph Theoretic Approach for Approximating the Heat Flux in Additive Manufacturing

2.1. Background and Prior Related work in Graph Theory

Our aim is to solve the so-called heat equation, as it appears hereunder, using a discrete graph theoretic approximation approach.

$$\frac{\partial T}{\partial t} - \alpha\left(\frac{\partial^2 T}{\partial x^2} + \frac{\partial^2 T}{\partial y^2} + \frac{\partial^2 T}{\partial z^2}\right) = 0 \tag{1}$$

In the heat equation, $T(x, y, z, t)$ refers to the temperature, t is the time, and *x, y,* and *z* the Cartesian spatial coordinates for a given part geometry. From the AM perspective, the term $\partial T/\partial t$ is analogous to the rate of change temperature at a particular point in the part referenced by its coordinates (*x, y, z*) as it is heated by a moving energy source while being completed layer-upon-layer, e.g., a laser in LPBF. Representing the continuous Laplacian operator $\boldsymbol{\Delta}(T) \stackrel{\text{def}}{=} \left(\frac{\partial^2}{\partial x^2} + \frac{\partial^2}{\partial y^2} + \frac{\partial^2}{\partial z^2}\right) T$, the heat equation reduces to,

$$\frac{\partial T}{\partial t} - \alpha\boldsymbol{\Delta}(T) = 0 \tag{2}$$

The graph theoretic approach for solving the heat equation of Eqn. (1) is based on discretizing the continuous Laplacian operator $\boldsymbol{\Delta}$, by a weighted and undirected graph over a grid of points (nodes) sampled within the geometry of the part. The continuous Laplacian operator $\boldsymbol{\Delta}$ is then approximated by a discrete Laplacian operator (L) called the graph Laplacian Matrix. As we will show in the forthcoming section (Sec. 2.3), the discrete Laplacian L allows for solutions of the heat equation to be constructed from its eigenvectors (ϕ) and eigenvalues (Λ), which are found by well-established computational methods; the solution takes the form,

$$T(x, y, z, t) = e^{-\alpha(\phi \mathrm{L} \phi')} = \phi e^{-\alpha \Lambda t} \phi' \tag{3}$$

A review paper by Solomon [12] discusses discrete differential operators that arise from partial differential equations (PDEs) such as the heat equation; it shows that the Laplacian matrix constructed from a uniformly-spaced grid gives a solution to the heat equation. However, if the grid is not equally spaced, the relationship to the correct solution of the heat equation is not clear. In a study of geometric surface smoothing, Belkin *et al.* [13] assert that their

discrete Laplacian matrix approaches the continuous Laplacian in the limit as the grid become sufficiently fine, even if the grid pattern is non-uniform. Their algorithm includes multiplicative factor $1/h^2$ where h which is the size of the neighborhood of influence for nearby grid points. In a study of image smoothing, Zhang and Hancock use randomly-assigned node locations to construct a discrete Laplacian matrix and subsequently to solve the heat equation [14]. The approach of Zhang and Hancock is used in Sec. 2.3 for the calculations reported in this paper [14]. We note that our approach is distinct from the mesh-free methods developed for peridynamics of systems undergoing dynamic cracking [15, 16] and it is also different from spectral collocation methods where splines provide an a priori functional form of the solution as part of a standard matrix-inversion process [17].

2.2. Modeling the heat flux in AM as a spectral graph theoretic problem

To keep the development brief, the following simplifying assumptions are applied to the graph theoretic approach.

- The laser rays are completely absorbed in the topmost layer and are not repeatedly reflected by the powder.
- The part boundary is completely insulated, and no heat is lost on account of convective heat transfer.
- The laser in LPBF and DED is considered a moving heat source that is focused at a single point, i.e., the beam diameter and shape, and subsequent diffusion on the powder bed surface are not accounted.
- The time required by the laser to fuse a layer is infinitesimal compared to the time taken to deposit a new layer. Hence, heat dissipation occurs only during the powder deposition process as the bed is lowered and the recoater applies a new layer.

These assumptions can provide a more comprehensive model, which will be pursued in later works by the authors.

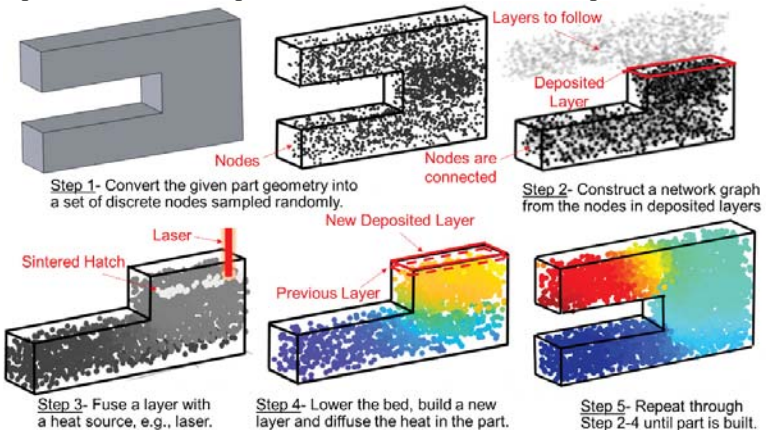

Figure 1. The five steps in the spectral graph theoretic approach used to estimate the heat flux in the part layer-by-layer. Here we show an embodiment of the laser powder bed fusion (LPBF) process.

The approach has the following five steps, as shown in Figure 1.

Step 1: Graph Embedding - Constructing a network graph from the nodes as a layer is deposited by the recoater.

The part is sliced into layers and hatches, and a fixed number of spatial locations (nodes) which are randomly sampled. The number of nodes is contingent on the geometry of the part, in this work, a density of 5 nodes per mm^2 provided a sufficiently good approximation to the heat flux estimated with a moving heat source solution obtained through FEA [18, 19].

Step 2: Constructing a network graph from the nodes as a layer is deposited by the recoater.

We begin by constructing a graph over the set of nodes sampled in Step 1. The aim is to connect a pair of nodes π_i and π_j within an ε neighbourhood per a kernel function Ω. The nodes are indexed by their spatial coordinates (*x,y,z*) in the part. In other words, if we take the pairwise distance between any two nodes π_i and π_j via the function Ω, this is expressed in mathematical terms as below, with Gaussian radial basis function Ω.

$$a_{ij} = \begin{cases} e^{-\frac{(\pi_i - \pi_j)^2}{\sigma^2}}, & (\pi_i - \pi_j)^2 \leq \epsilon \\ 0, & (\pi_i - \pi_j)^2 > \epsilon \end{cases} \tag{4}$$

where $(\pi_i - \pi_j)^2$ is the square of the distance between nodes π_i and π_j. The matrix formed of a_{ij} is called the adjacency matrix, A. In this work, the term ϵ is akin to the radius of a sphere within which all nodes are connected, and σ is the standard deviation of the pairwise distances.

$$\mathrm{A} = [a_{ij}] \tag{5}$$

The matrix A is symmetric and sparse. The next step involves computing the degree d_i of a node i, i.e., the number of edges that are connected to the node i. The degree of node π_i is computed by summing each row of the Adjacency matrix A,

$$d_i = \sum_{\forall j} a_{ij} \tag{6}$$

From the degree of node d_i, the Laplacian l_{ij} at node i is defined as follows,

$$l_{ij} \stackrel{\text{def}}{=} d_i - a_{ij} \tag{7}$$

We note that $\sum_{\forall j} l_{ij} = 0$; if the diagonal degree matrix D is formed as follows, $\mathrm{D} \stackrel{\text{def}}{=} \mathrm{diag}(d_1, \cdots, d_M)$. Then given adjacency matrix A, the discrete Laplacian L can be cast in matrix form as,

$$\mathrm{L} \stackrel{\text{def}}{=} (\mathrm{D} - \mathrm{A}) \tag{8}$$

Finally, the Eigen spectra of the Laplacian L is computed; $\mathrm{L}\phi = \Lambda\phi$.

Step 3: Simulating the fusion of each layer hatch-by-hatch.

The heat is applied to the powder bed in the form of linear hatches. The magnitude of heat applied is indexed as $H(x,y,z)$. Where the time taken to fuse a layer is considered infinitesimal compared to the time it takes the bed to be lowered and to the recoater to deposit a new layer. For practical application in LPBF or DED, $H(x,y,z)$ is the initial condition, and it can be considered as a volumetric energy density in Joules/mm^3 applied at a particular volume. The volumetric energy density is given by $\mathrm{E}_V = \frac{\mathrm{P}}{\mathrm{h}\cdot\mathrm{v}\cdot\mathrm{t}}$ J/mm^3, where P is the laser power in Watts, h is the distance between adjacent passes of the laser (called hatch spacing, mm), v is the velocity of the laser in mm/s, and t is the layer height (mm).

Step 4: Estimating the heat from diffusion and building up the next layer.

The heat diffuses to the rest of the part within the powder bed, and through the substrate in the time t it takes to lower the bed and deposit material. As we will show in the forthcoming two sections, the eigenvectors ϕ of the Laplacian L provide a discrete solution to the heat equation, specifically, if ϕ' is the transpose of ϕ, then the temperature profile at time step τ for a node at position (x, y, z) is given by the following [14],

$$T(x,y,z,t) = H(x,y,z)e^{-\alpha(\phi' \mathrm{L}\phi)t} \tag{9}$$

Where the material-related factors are contained in the term α. Finally, in Step 5 we estimate the heat flux across layers by repeating Steps 2 through 4 until the part is built.

Step 5: Steps 2 through 4 are cycled until the process is completed.

2.3. Justification for using the Eigenvectors and Eigenvalues of the Graph Laplacian to Solve the Heat Equation

Consider the heat equation $\frac{\partial T}{\partial t} - \alpha\boldsymbol{\Delta}(T) = 0$, for separation of variables, letting,

$$T(r,t) = R(r)\theta(t) \Rightarrow \frac{1}{\alpha}R\frac{\partial\theta}{\partial t} = \boldsymbol{\Delta}(R)\theta \Rightarrow \frac{1}{\alpha\theta}\frac{\partial\theta}{\partial t} = \frac{\boldsymbol{\Delta}(R)}{R} \tag{10}$$

The above equation shows that a function of time is equal to a function of space, which can only be true if both are equal to a collection of constants Λ called eigenvalues. That is,

$$\frac{1}{\alpha\theta}\frac{\partial\theta}{\partial t} = \frac{\boldsymbol{\Delta}(R)}{R} = -\Lambda \tag{11}$$

Consider the spatial portion of the above equations,

$$\boldsymbol{\Delta}(R) = -\Lambda R \tag{12}$$

The above is called the Helmholtz equation; multiply both sides by θ,

$$\boldsymbol{\Delta}(R)\theta = -\Lambda R\theta \Rightarrow \boldsymbol{\Delta}(T) = -\Lambda(T) \tag{13}$$

That is the temperature also satisfies the Helmholtz equation $\boldsymbol{\Delta}(T) = -\Lambda(T)$, where Λ are the eigenvalues corresponding to their eigenfunctions ϕ of the Laplacian. As a consequence, we have,

$$\frac{\partial T}{\partial t} - \alpha[\boldsymbol{\Delta}(T)] = 0 \Rightarrow \frac{\partial T}{\partial t} + \alpha\big(\Lambda(T)\big) = 0 \tag{14}$$

For the Neumann, Robin, and Dirichlet boundary conditions, it is shown by Saito that the eigenvalues (Λ) of the Laplacian operator are discrete and non-negative, and the eigenfunctions (eigenvectors) are orthogonal, i.e., $\langle \phi_i, \phi_j \rangle = \mathbf{0}$, assuming that the domain Ω of the Laplacian is bounded, connected and compact [20]. Hence, the key

idea for solving the heat equation of Eqn. (1) is to discretize the continuous Laplacian operator $\boldsymbol{\Delta}$ can be discretized in terms of a the Laplacian Matrix L over a grid laid over the part.

If the grid is defined in a way such that when its points (vertices or nodes) are connected with edges, the resulting adjacency matrix A in Eqn. (5) is real, and therefore its Laplacian matrix (L), Eqn. (8) is diagonally dominant and symmetric, i.e., semidefinite positive semidefinite. Hence, the orthogonality of Eigenvectors and non-negativity of eigenvalues is preserved. Furthermore, because the transpose of an orthogonal matrix is the same as its inverse, i.e., $\phi^{-1} = \phi'$, and $\phi\,\phi' = \mathrm{I}$, hence, $\Lambda = \phi \mathrm{L} \phi'$. On substituting the foregoing into the Helmholtz equation $\boldsymbol{\Delta}(T) = -\Lambda(T)$, we obtain $-\boldsymbol{\Delta}(T) = \phi \mathrm{L} \phi'(T)$. Plugging the last relationship into the heat equation (Eqn. (1)) and solving the partial differential equation– consider a unit heat source is applied, i.e., $H(x, y, z) = 1$, we obtain,

$$\frac{\partial T}{\partial t} + \alpha(\phi \mathrm{L} \phi')(T) = 0 \Rightarrow T(x, y, z, t) = e^{-\alpha(\phi \mathrm{L} \phi')} \tag{15}$$

This formal solution will be simplified by considering the Taylor Series expansion of the term $e^{-\alpha(\phi \mathrm{L} \phi^{\mathrm{T}})}$, and substituting, $\phi\,\phi' = \mathrm{I}$ and $\mathrm{L}\phi = \Lambda\phi$, as shown by Zhang *et al.* and Bai *et al.* as follows [14, 21],

$$\begin{aligned} e^{-\alpha(\phi \mathrm{L} \phi^{\mathrm{T}})} &= 1 + \frac{(-\alpha(\phi \mathrm{L} \phi')t)}{1!} + \frac{(-\alpha(\phi \mathrm{L} \phi')t)^2}{2!} + \frac{(-\alpha(\phi \mathrm{L} \phi')t)^3}{3!} + \cdots \\ &= 1 - \alpha t \frac{\phi \Lambda \phi'}{1!} + \alpha^2 t^2 \frac{(\phi \Lambda \phi')(\phi \Lambda \phi')}{2!} - \alpha^3 t^3 \frac{(\phi \Lambda \phi')(\phi \Lambda \phi')(\phi \Lambda \phi')}{3!} + \cdots \\ &= 1 - \frac{\phi \Lambda \alpha t \phi'}{1!} + \frac{\phi (\Lambda \alpha t)^2 \phi'}{2!} - \frac{\phi (\Lambda \alpha t)^3 \phi'}{3!} + \cdots \\ e^{-\alpha(\phi \mathrm{L} \phi')} &= \phi e^{-\alpha \Lambda t} \phi' \end{aligned}$$

$$\therefore T(x, y, z, t) = e^{-\alpha(\phi \mathrm{L} \phi')t} = \phi e^{-\alpha \Lambda t} \phi' \tag{16}$$

Thus, the heat equation is solved as a discrete function of the eigenvectors and eigenvalues of the graph Laplacian L.

3. Verification of the Approach with a Finite Element Method based on Goldak's Moving Heat Source Model.

Goldak *et al.* considered a 3D moving heat source model with an ellipsoidal, Gaussian density distribution [18, 19]. Goldak's model has been adapted for thermal modeling in additive manufacturing process, e.g., LPBF with the laser is considered a 3D Gaussian distributed moving heat source [22]. We use Goldak's model in an FEA framework (Abaqus) with an element birth-and-death technique to simulate the LPBF process; the DFLUX subroutine is leveraged to model the characteristics of the laser. The Gaussian distributed laser heat source is defined as,

$$Q(x, y, z) = \frac{PA}{2\pi\sigma^2} \exp\left[-\frac{d^2}{2\sigma^2}\right] \tag{17}$$

Where, Q is the volume heat power density (J/m^3), P is the laser power (W), A is the absorptivity constant, σ is the standard deviation ($\sigma = D/4$ which D is the beam diameter in mm) and d (mm) is the radial distance of a point from the center of the beam. In this mode, conduction plays the main role in transferring the applied heat through the part and substrate. The simplest form of the transient heat conduction equation is used in this study.

$$\rho C_p \frac{\partial T}{\partial t} - k\boldsymbol{\Delta} T = Q(x, y, z) \tag{18}$$

In the above, ρ is the density, C_p is the specific heat of the material, T is the temperature, t is time and k is the thermal conductivity. A portion of the applied heat will be lost through the convection, radiation and surface evaporation which is not considered in this study.

3.1. Description of the Boundary Conditions used for the Moving Heat Source Finite Element Model

The LPBF of a C-shape part (Figure 2(a)) is simulated on top of a build plate with the dimension of 100 × 20 × 10 mm. The titanium alloy powder material Ti-6Al-4V is considered for both the part and the build plate. Figure 2 shows the dimension, top-view (a), side-view (b), and scanning strategy (c) used in the LPBF simulation. The hatches are defined along y-axis and layers along z-axis. The laser was simulated to move along x-axis and fused 4 hatches in each layer. Hatch thickness and layer thickness are 0.5 mm. The material properties are reported in Table 1. The initial temperature is assumed to be the ambient temperature for the entire build, i.e., $T(x, y, z, \tau)_{\tau=0} = T_{amb.} = 25$ °C, and the boundary surfaces are considered to be perfectly insulated. Hence no heat is transferred from the part to the atmosphere except to the build plate, which is assumed as a heat sink.

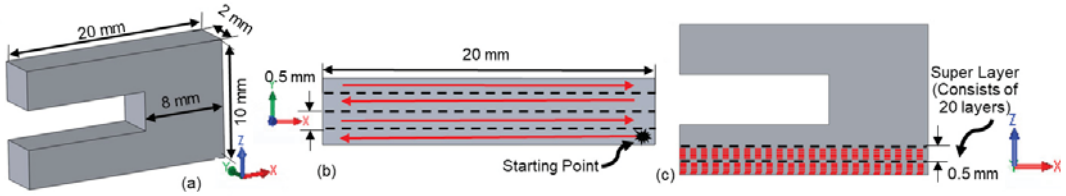

Figure 2. (a) Dimension of C-shape part in mm, (b) top view of C-shape part and scanning strategy in simulation, (c) side view of C-shape part.

Table 1. Materials and Process Parameters for the FEA simulation

Parameters	Values	Parameters	Values
Layer Thickness (mm)	0.025	Beam Diameter (mm)	0.5
Super-Layer Thickness (mm) (included 20 layers)	0.5	Thermal Conductivity (W/m-K)	20
Hatch thickness (mm)	0.5	Density (kg/m^3)	4300
Scanning Speed (mm/s)	200	Specific Heat (J/kg-K)	650

3.2. Comparison of Heat Flux Results from Finite Element Analysis with Graph Theory

The C-shaped part was simulated layer-by-layer using the proposed graph theoretic approach. The parameters were set as follows, $\alpha = 15$; $\epsilon = 1.8$ mm; and 50 nodes are sampled per hatch which translates to 5 nodes per mm^2. The result from the last step (layer) of the FEA and graph theoretic simulations is juxtaposed pictorially in Figure 3; the color bars represent normalized temperature between 0 and 1. Figure 3 shows that the temperature distribution captured by the graph theoretic approach closely resembles those derived from the FEA. The temperature at two locations on the bottom of the part were recorded over the complete simulation run, analogous to the presence of thermocouple sensors affixed to the part. These two measurement points are at a distance of 1 mm from the left edge and 1 mm from the right edge of the part, respectively, as demarcated in the inset of Figure 3(c) and (d), and are located 1 mm deep from the front edge of the part. We observe that the trends obtained from Figure 3(c) and (d) for both the FEA- and graph-based methods are closely correlated. More pertinently, the simulation time for the FEA approach (Abaqus) was close to 200 minutes on a dual cores of Intel® Core™ i7-6700 CPU @3.40GHz, while the computation time for the graph theoretic approach was less than 200 seconds (Matlab). In Figure 3(a) and (b) the overhang geometry is observed to have a higher magnitude of constrained heat. The temperature trends observed in Figure 3(c) and (d) is explained on partitioning the part geometry into three sections T1 through T3 as demarcated in Figure 3(a).

- In Figure 3 (c) the spikes in section T1 correspond to the locations where the laser is directly above the position of the measurement point (sensor). In section T2, the laser no longer passes over the location of the sensor leading to the observed precipitous drop. In section T3, given the impeded conductivity of the powder surrounding the overhang, the temperature does not increase.
- In Figure 3 (d), the spikes in section T1 correspond to the location where the laser passes over the sensor position. In part section T2, the increase in temperature can be attributed to two reasons: (a) in this section of the laser passes frequently and directly above the sensor location, and (b) the section is surrounded by a large volume of powder that hinders the flow of heat. Lastly, in section T3, the temperature begins to rise again due to the constrained heat flux in the overhang feature.

3.3. Effect of Part Design on the Heat Flux

It was hypothesized that designing supports (under the overhang) would provide a pathway for the heat to dissipate into the build plate. Accordingly, the C-shaped part was modified as shown in Figure 4(a). The build process used the identical settings for the FEA and graph-theoretic approach described in previous sections, Sec. 3.1 and Sec. 3.2. The simulated heat flux trends are summarized hereunder.

- The heat flux on the melting of the last layer with the FEA and graph theoretic approach are shown in Figure 4(b) and (c), respectively. The trends therein affirm the hypothesis that placing supports with a thick cross section leads to dissipation of heat that is constrained within the overhang section.
- Likewise juxtaposing Figure 4(d) and (e) against, Figure 3(b) and (c), respectively, it is evident that placing the supports under the overhang section diminishes the steep thermal gradients when transitioning from across the different sections of the part. As a consequence, the possibility of thermal stress-related deformation and cracking are potentially minimized.

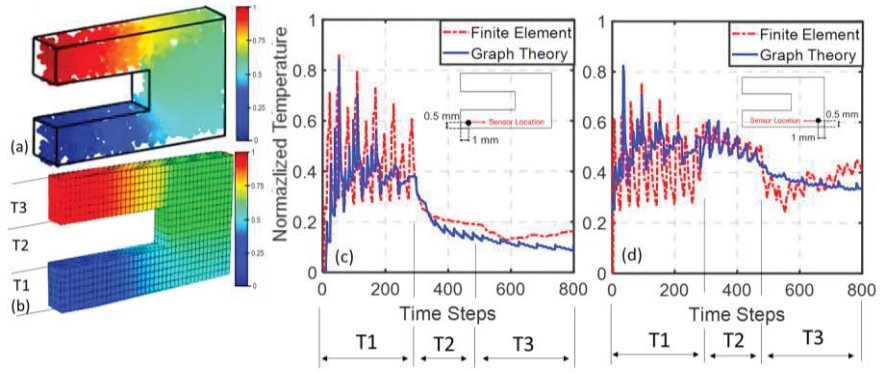

Figure 3. (a) and (b) The heat flux during melting of the last layer estimated using the graph theoretic, and finite element-based approach respectively. (c) and (d), the heat flux trends observed at two locations on the part, in the left and right corner, respectively corresponding to the three-part sections marked in (b).

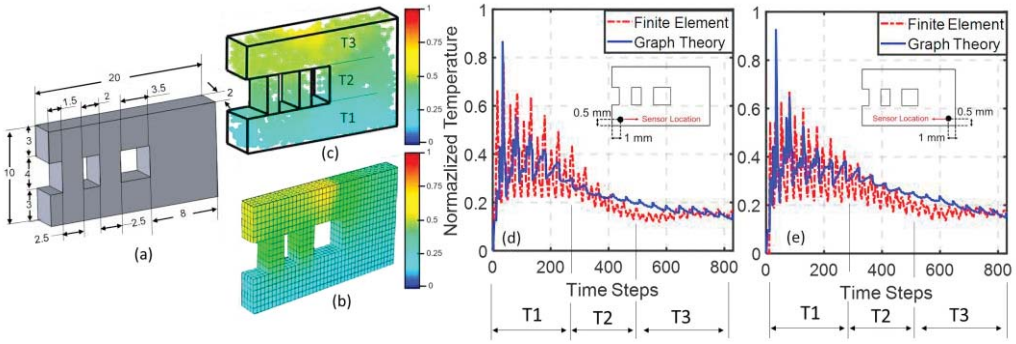

Figure 4. (a) The C-shaped part from Figure 3 is modified with two supports to provide a path for the heat in the overhang section to dissipate. (b) and (c) The heat flux during fusion of the last layer of the modified part with two supports specially designed estimated using the graph theoretic, and finite element-based approach respectively. (d) and (e), the heat flux trends observed at two locations on the part, in the left and right corner, respectively, corresponding to the three sections marked in (c).

4. Conclusions and Avenues for Future Work

We developed and applied a new graph theoretic approach to understand the direction and magnitude of heat flow (heat flux) in metal AM processes. Specific conclusions from this work are as follows.

- Laplacian eigenvectors and eigenvalues of the graph embedded onto the geometry of the part solves the heat equation. In other words $T(x,y,z,\tau) = e^{-\alpha(\phi L \phi')t} = \phi e^{-\alpha \Lambda t}\phi'$, where ϕ and Λ are the eigenvectors and eigenvalues of the Laplacian matrix (L) representing the graph embedded in a part geometry.
- The above mathematical result is used to simulate a LPBF process, and the results are compared with finite element analysis (FEA) moving heat source model based on the work of Goldak [18, 19]. The discrete approximation of the heat flux trends obtained using the graph Laplacian eigenvectors and eigenvalues is observed to closely correlated with results from the FEA-based approach.
- The computation time to estimate the heat flux with the graph theoretic approach for the two test parts studied was less than 3 minutes (Matlab). In contrast, the FEA-based approach (Abaqus) took over 3 hours.

While this work presents the first foray into using graph theory for modeling the part-level phenomena in metal AM, several questions remain to be answered, which we will endeavor to resolve in our forthcoming works.

1) What is the effect of the process parameters on the heat flux and part deformation?
2) What is the accuracy of the approach both in terms of exact thermal solutions, such as those obtained from a Green's functions, and experimental validation with metal AM processes?

References

[1] Schmidt, M., Merklein, M., Bourell, D., Dimitrov, D., Hausotte, T., Wegener, K., Overmeyer, L., Vollertsen, F., and Levy, G. N., 2017, "Laser based additive manufacturing in industry and academia," CIRP Annals, 66(2), pp. 561-583.

[2] Sames, W. J., List, F. A., Pannala, S., Dehoff, R. R., and Babu, S. S., 2016, "The metallurgy and processing science

of metal additive manufacturing," International Materials Reviews, 61(5), pp. 315-360.
[3] Seifi, M., Salem, A., Beuth, J., Harrysson, O., and Lewandowski, J. J., 2016, "Overview of Materials Qualification Needs for Metal Additive Manufacturing," JOM, 68(3), pp. 747-764.
[4] Montazeri, M., and Rao, P., 2018, "Sensor-Based Build Condition Monitoring in Laser Powder Bed Fusion Additive Manufacturing Process Using a Spectral Graph Theoretic Approach," Journal of Manufacturing Science and Engineering, 140(9), pp. 091002-091002-091016.
[5] Montazeri, M., Yavari, R., Rao, P., and Boulware, P., 2018, "In-Process Monitoring of Material Cross-Contamination Defects in Laser Powder Bed Fusion," Journal of Manufacturing Science and Engineering, 140(11), pp. 111001-111001-111019.
[6] Imani, F., Gaikwad, A., Montazeri, M., Rao, P., Yang, H., and Reutzel, E., 2018, "Process Mapping and In-Process Monitoring of Porosity in Laser Powder Bed Fusion Using Layerwise Optical Imaging," Journal of Manufacturing Science and Engineering, 140(10), pp. 101009-101009-101014.
[7] Malekipour, E., and El-Mounayri, H., "Defects, Process Parameters and Signatures for Online Monitoring and Control in Powder-Based Additive Manufacturing," Springer International Publishing, pp. 83-90.
[8] Amini, M., and Chang, S. I., 2018, "MLCPM: A process monitoring framework for 3D metal printing in industrial scale," Computers & Industrial Engineering, 124, pp. 322-330.
[9] DebRoy, T., Wei, H. L., Zuback, J. S., Mukherjee, T., Elmer, J. W., Milewski, J. O., Beese, A. M., Wilson-Heid, A., De, A., and Zhang, W., 2018, "Additive manufacturing of metallic components – Process, structure and properties," Progress in Materials Science, 92, pp. 112-224.
[10] Zeng, K., Pal, D., Gong, H. J., Patil, N., and Stucker, B., 2015, "Comparison of 3DSIM thermal modelling of selective laser melting using new dynamic meshing method to ANSYS," Materials Science and Technology, 31(8), pp. 945-956.
[11] Denlinger, E. R., 2018, "Chapter 12 - Development and Numerical Verification of a Dynamic Adaptive Mesh Coarsening Strategy for Simulating Laser Power Bed Fusion Processes," Thermo-Mechanical Modeling of Additive Manufacturing, M. Gouge, and P. Michaleris, eds., Butterworth-Heinemann, pp. 199-213.
[12] Solomon, J., 2015, "PDE approaches to graph analysis," arXiv preprint arXiv:1505.00185.
[13] Belkin, M., Sun, J., and Wang, Y., "Discrete laplace operator on meshed surfaces," Proc. Proceedings of the twenty-fourth annual symposium on Computational geometry, ACM, pp. 278-287.
[14] Zhang, F., and Hancock, E. R., 2008, "Graph spectral image smoothing using the heat kernel," Pattern Recognition, 41(11), pp. 3328-3342.
[15] Silling, S. A., and Askari, E., 2005, "A meshfree method based on the peridynamic model of solid mechanics," Computers & Structures, 83(17), pp. 1526-1535.
[16] Chen, Z., Niazi, S., Zhang, G., and Bobaru, F., 2017, "Peridynamic Functionally Graded and Porous Materials: Modeling Fracture and Damage," Handbook of Nonlocal Continuum Mechanics for Materials and Structures, G. Z. Voyiadjis, ed., Springer International Publishing, Cham, pp. 1-35.
[17] Sun, Y.-S., and Li, B.-W., 2010, "Spectral Collocation Method for Transient Conduction-Radiation Heat Transfer," Journal of Thermophysics and Heat Transfer, 24(4), pp. 823-832.
[18] Goldak, J. A., and Akhlaghi, M., 2005, "Computer simulation of welding processes," Computational Welding Mechanics, pp. 16-69.
[19] Goldak, J., Chakravarti, A., and Bibby, M., 1984, "A new finite element model for welding heat sources," Metallurgical Transactions B, 15(2), pp. 299-305.
[20] Saito, N., 2013, "Tutorial: Laplacian Eigenfunctions - Foundations and Applications," University of California, Davis, Graduate University for Advanced Studies, National Institute of Fusion Science, Japan.
[21] Bai, X., and Hancock, E. R., "Heat Kernels, Manifolds and Graph Embedding," Springer Berlin Heidelberg, pp. 198-206.
[22] Karayagiz, K., Elwany, A., Tapia, G., Franco, B., Johnson, L., Ma, J., Karaman, I., and Arróyave, R., 2018, "Numerical and experimental analysis of heat distribution in the laser powder bed fusion of Ti-6Al-4V," IISE Transactions, pp. 1-17.

Acknowledgements

One of the authors (PKR) thanks the National Science Foundation for funding his work through Grant Nos. CMMI-1719388, 1739696, and 1752069. Specifically, the development and application of graph theoretic approaches for process modeling and monitoring in metal AM processes presented in this paper was conceptualized and funded through CMMI-1752069 (CAREER).